Colored radiative cooling coatings with fluorescence

Refet Yalçın, Etienne Blandre, Karl Joulain, Jérémie Drevillon

Colored Radiative Cooling Coatings with Fluorescence

Refet Ali Yalçın,[a,*] Etienne Blandre,[a] Karl Joulain,[a] Jérémie Drévillon[a]
[a] Institut Pprime, CNRS, Université de Poitiers, ISAE-ENSMA, F-86962 Futuroscope Chasseneuil, France

Abstract. We propose structures that are colored with photoluminescence materials for radiative cooling applications. Using simulations, we show that implementing photoluminescence materials provides color to the structures by shifting electromagnetic energy between spectrums. Resulting additional solar energy absorption due to coloration is lower with photoluminescence compared to the traditional materials used for spectrally selective absorption such as pigments and nano-sized metallic resonators. Thermal and visual performance of different type of photoluminescence materials such as phosphors and quantum dots are investigated. Effects of Stokes shift and quantum yield, which are the photoluminescence properties that characterize the energy shift between spectrums, are quantified.

Keywords: optics, radiative cooling, fluorescence, phosphor, quantum dot, color, aesthetic, Monte Carlo method.

***Fourth Author, E-mail: refetyalcin@ucla.edu

1 Introduction

It is well known that objects at different temperatures can exchange radative energy through transparent or semi-transparent media. For example, a heated object exposed to sky can cool down by directly exchanging radiation with outer space at 3 K through the [8 µm - 12 µm] IR atmosphere transparent window. This is the so-called radiative cooling1 which is particularly efficient when the heated object is highly emissive in this transparent window. Such a radiative cooling can also be effective during daylight providing the considered object surface is highly reflective or non-absorbing in the solar spectrum while cooling in the IR. For radiative cooling commercial applications such as cars, product packages or buildings, the coatings considered have to present aesthetics as well as good thermal performances as seen in Figure 1. As the prism reveals, there are rainbow colors in the sunlight and since the colors are mixed, they look whitish to eye whose saturation is zero by definition. We see the objects after the light is reflected from the object. In order to obtain colored coatings, the balanced spectrum of light source should be disrupted. Generally, the disruptions are performed by pigments[2]. Metallic structures[3] and nanoparticles (NPs)[4] which can absorb a certain amount of light in the visible spectrum are also considered for

the photonic structures as the spectral location of absorption peak can be adjusted. Since absorption at a certain visible band contradicts with high solar reflectance requirement of the radiative coatings, these bands should be kept as narrow as possible by local resonances. For this purpose, in our former studies, we used silica core – silver shell nanoparticles[5] and metallic nanolayers[6] between dielectric layers. As an alternative to the metallic absorbers[3,7], Son et.al.[8] embedded photoluminescence materials to the radiative cooling coatings and obtained colorful structures that are capable of staying below ambient temperature under sunlight. Fluorescent particles disrupt the balance in the visible spectrum by both destructing one side of the visible spectrum with excitation and constructing another side with emission. Compared to the metallic resonators and non-fluorescent dyes which absorb the visible radiative energy and convert it to non-radiative form, using fluorescents are expected to be more suitable to introduce color not only to radiative cooling structures but also other designs that requires color and low solar absorptance together.

Phosphors absorb the incoming photons and re-emit them at other wavelengths. However, some of the absorbed photons are not re-emitted. They absorbed for good and transformed to non-radiative energy form. To quantify that portion, the term quantum yield (QY) is used which is defined as ratio of emitted photon number to absorbed photon number. For radiative cooling purposes, high QY is crucial to have a high thermal performance. Phosphors generally absorb at shorter wavelengths and emits at higher wavelengths which is called down-conversion. A spectral shift, named as Stokes shift is observed at down-converting phosphors. Magnitude of this shift is the distance between peaks of excitation and emission wavelengths. This shift also causes energy loss since the emitted photon's energy is lower than absorbed photon's energy. As the ratio between emission and excitation wavelength increases, energy loss due to Stokes shift increases

considering photon energy is $h \cdot c/\lambda$ where h is Planck constant, c is speed of light and λ is wavelength.

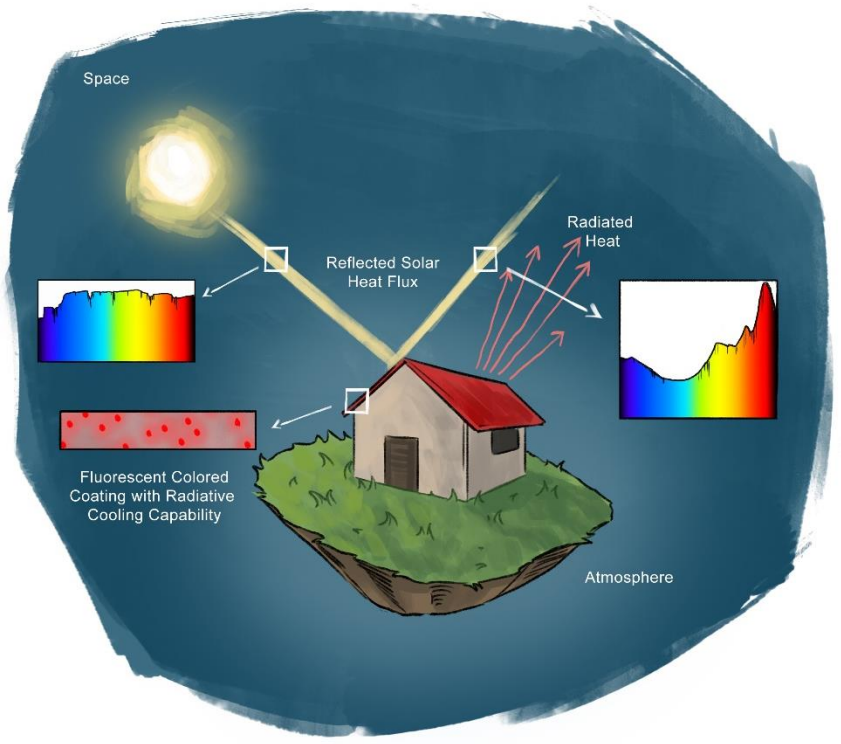

Figure 1 - Colored radiative cooling coating applied on the roof

In addition to micron sized phosphors, quantum dots with their a few nanometer sizes are used for photoluminescence. Unlike phosphors, their emission spectra can be altered easily by varying their size. Their quantum yields used to be only good at low temperatures[9,10], but a recent study[11] shows that high quantum yields up to 100% is also achievable at room temperatures. To have an efficient thermal performance, high quantum yield is more crucial for quantum dots than regular micron sized phosphors because emission bands of quantum dots overlap with absorption bands at a much wider range than regular micron sized phosphors. Emitted photon that are re-absorbed by the quantum dot will result lower thermal efficiency as quantum yield deviates more from unity. Due to their a few nanometer size, light scattering of quantum dots is in Rayleigh scattering regime

under solar spectrum and scattering cross-section of quantum dots are negligible compared to the absorption cross-section. Considering the typical refractive index value of 1.5 for thermal emitters around solar spectrum, the parallel plane air-coating interface has a critical angle around 42°. Rays that are incident wider than that angle, cannot leave the coating and total internal reflection occurs. Unlike fiber-optic cable, reflected rays do not travel a long distance in the proposed coatings with multiple reflections since the other side of emitter is not air but non-ideal metallic reflector as seen in Figure 2. Each reflection absorbs a few percent of the intensity and thermal performance drops. Considering photoluminescence is isotropic, the emitted light that arrives to interface wider than critical angle cannot leave the coating. As the quantum dots cannot scatter light like the micron sized phosphors do, scatterer nanoparticles can be embedded to the coating along with quantum dots to alter the direction of light and improve reflectance of the coating.

Radiative transfer equation is used to model radiative transfer within the coating. Monte Carlo method is a well-known method to solve radiative transfer equation (RTE) since its first application by Perlmutter and Howell[12]. Fluorescence in the medium can also be implemented to the RTE and solved by Monte Carlo method[13]. Application areas of the modified Monte Carlo method are included but not limited to lighting[14] and biomedical[15,16] research. In our previous paper[17] we showed that our open-source Monte Carlo solver[18] is capable of solving fluorescence in plain parallel medium by validating an experimental case. Same code is used in this study to find reflectance and absorptance of the fluorescent coatings.

This study numerically investigates the thermal and visual performance of the photoluminescent materials for colored radiative coatings. During the study we observe challenges that result in low thermal and optical performance while using quantum dots, low-absorbing fluorescent particles and obtaining blue colored coatings. We address solutions to these challenges for improving the

performances. We also quantify the effects of fluorescence properties such as Stokes shift and quantum yield on color and thermal performance of the radiative cooling structures. We compare the non-fluorescently colored coatings with fluorescent ones and identify the advantages and disadvantages of each type.

2 Problem Statement

A good reflection in the solar spectrum waveband and a good emittance in the atmospheric transmittance window are the well-known characteristics of an efficient daytime radiative cooling structure. For example, simple well-known efficient structure is the two layered design which is shown in Figure 2 where a good solar reflective metallic bottom layer is covered with a spectrally selective material which absorbs weakly in solar spectrum and emits efficiently in the infrared spectrum. Here, we compare two different well-known emitters namely SiO2 (silica) and Polydimethylsiloxane (PDMS) forradiative cooling structures. Then, we investigate the cases in which the emitter is embedded with fluorescent materials whose excitation and emission spectrum are presented in Figure 3 (a) and (b) respectively.

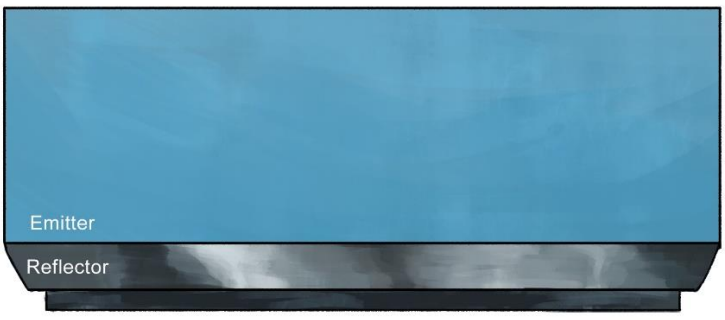

Figure 2 - Sketch of the simple two-layer coating

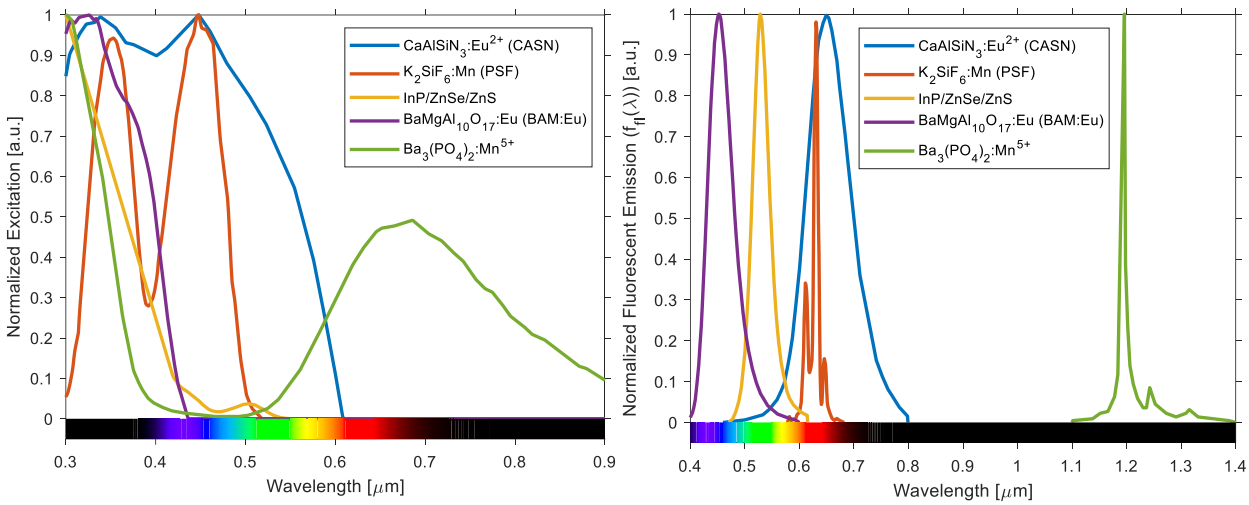

(a) (b)

Figure 3 – (a) Excitation and (b) emission spectrum of the CASN[19], PSF[20], InP/ZnSe/ZnS[21], BAM:Eu[22] and $Ba_3(PO_4)_2:Mn^{5+}$[23].

2.1 IR Emitter

200 nm thick silver is chosen as the metallic reflective layer which has suitable optical properties[24] for solar reflection whereas two different materials; silica (SiO2) and polydimethylsiloxane (PDMS) are used as the emitters in the study. Silica has a lower solar absorptance than PDMS whereas emittance of PDMS at atmospheric window is better than silica. Depending on the application, one can outperform the other. Net radiative cooling of silver reflector - PDMS emitter and silver reflector - silica emitter coatings are studied for a wide range of thickness from 1 µm to 10 cm. As the spectrally selective emitter gets thicker, it emits better. On the other hand, solar absorption also increases with the increasing thickness which effects the cooling performance adversely. These contradictory behaviors of increasing thickness on radiative cooling power, would result an optimum thickness which is investigated in the study. The refractive index of silica and PDMS are taken from[25,26] respectively.

2.2 Weakly absorbing phosphors

A 5µm sized red phosphor $K_2SiF_6:Mn^{4+}$ (PFS) that is known with its high QY (92%)[27] but low absorbing characteristic[27] and refractive index[28] is used in the study to observe effect of binders (emitters). Its. Sketch of the coating is presented in Figure 4. Phosphor particles are not as absorptive as metallic NPs. Weakly absorbing PFS creates a challenge in structure design when high saturation is desired. PFS is embeddable to both polymers and silica[29]. Its performance in two different binders at various thicknesses is studied. We know that use of Monte Carlo method is valid as long as the concentration increase is linearly proportional to extinction coefficient. Since we know the relation is linear at least up to 20%[20] we chose the volume fraction (f_v) of all the coatings in this study 20% unless otherwise stated.

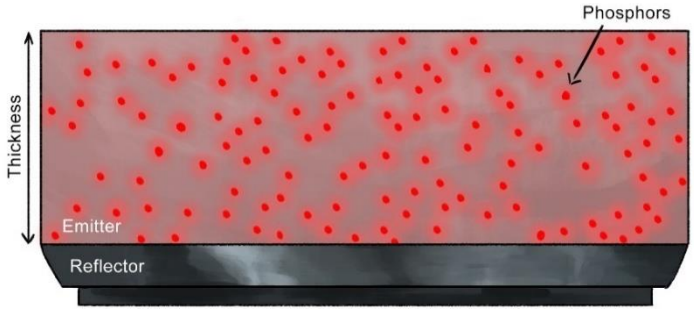

Figure 4 - Sketch of the simple two-layer coating embedded with phosphor

2.3 Down-converting phosphors

Micron sized $CaAlSiN_3:Eu^{2+}$ (CASN) which is a well-known good absorbing[20] phosphor that can easily be implemented in polymers is studied along with the colored coatings embedded with metallic NPs. CASN has a wide excitation spectrum and high quantum yield (96%)[19] which results in a promising visual and thermal performance. Particle size 7.5 µm and refractive index 2 is taken from[20]. The thermal and visual performance of the fluorescent coating is investigated along with the colored coating with silver NPs from[5] which has a mixture of plain silver NPs with diameter

$D = 50\ nm$ at $f_v = 30x10^{-6}$ and silica core, silver-shell NPs with outer diameter $D_o = 24\ nm$, inner diameter $D_i = 17\ nm$ at $f_v = 20x10^{-6}$.

2.4 Quantum dots

As quantum efficiency of quantum dots increases, they become more popular for numerous utilizations. Observing their effect on colored radiative cooling structures could reveal another possible application area. In this study, green emitting InP/ZnSe/ZnS shell-core-core quantum dot with $QY = 95\%$[21] is used. Its outer diameter is 7.3 nm ± 1.2 and for realistic modeling, wider emission spectrum[30], that considers the ensemble of quantum dot size distribution is used. Since it has a high molar extinction coefficient[31], PDMS is chosen as the emitter. As mentioned earlier, they cannot scatter light efficiently due to their small size compared to the wavelength. Scatterers are therefore also embedded as shown in Figure 5 to enable the escape of rays that are emitted with angles wider than the critical angle. Similar to QY term for fluorescent particles in terms of efficiency, single scattering albedo (ω_0) is important for scattering particles which is the ratio of scattering cross-section to extinction cross-section. Its formulation is given in[5] and is not repeated here for brevity. The spectral region of interest for absorption of the scatterers is solar spectrum since we want scattering albedo to be high at that range. Therefore, a weighted average albedo over solar spectrum is calculated where $I_{solar,\lambda}$ is the spectral solar intensity as:

$$\omega_s = \frac{\int_0^\infty \omega_{0,\lambda} I_{solar,\lambda} d\lambda}{\int_0^\infty I_{solar,\lambda} d\lambda} \quad (1)$$

Solar spectrum averaged scattering albedo of spherical TiO_2 and ZnO particles at different radii are investigated and their results are presented in Figure 6. Optimal TiO_2 particle radius is found

to be aroun 50 nm for the application. The amount of scatterer is expected to be changed with respect to quantum dot amount which is given in molarities. Therefore, a parametric study for the 100 µm thick PDMS coatings with two variables, namely concentrations of quantum dot and scatterer is studied to determine their effect on thermal and visual performance.

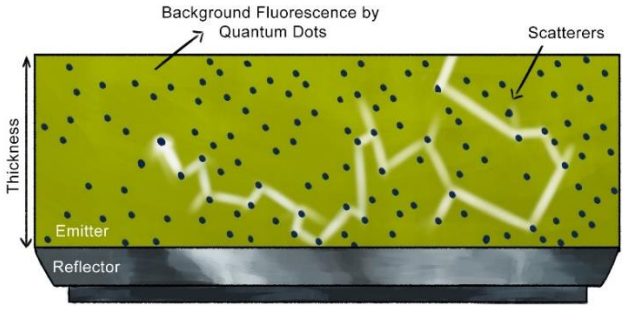

Figure 5 - Sketch of the two-layer coating with scatterer and quantum dots along with tracing of a ray emitted by quantum dot.

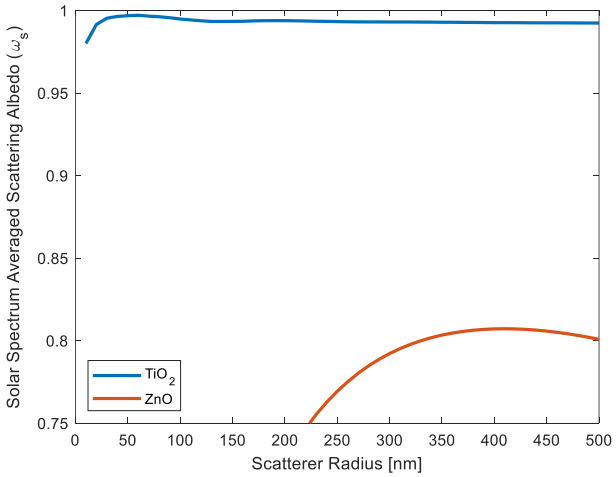

Figure 6 – Solar spectrum averaged single scattering albedo of TiO_2 and ZnO particles in PDMS.

2.5 Conversion between non-visible and visible spectrums

As we mentioned before, one of the reasons that we expect to observe high thermal and visual performance for colored radiative cooling structures with phosphors is that they can disrupt the visible spectrum not only by absorption but also by fluorescent emission. However, not all the phosphors have excitation and emitting bands that fall in the visible spectrum. Using a high QY

(90%)[22] phosphor such as $BaMgAl_{10}O_{17}$:Eu (BAM:Eu) that is absorbing in the UV and emitting in the visible could be beneficial for thermal performance since absorptance of the silver reflector in the UV range is high as it could be observed from Figure 7(b). Converting this spectrum of light into a wavelength range where silver is more reflective before reaching the reflective layer could improve thermal performance and also add coloration to the coating.

It is challenging to observe certain colors like blue and green under sunlight since the presence of other spectrums such as yellow and red suppress the blue and the coating would look yellowish or whitish. Since we cannot utilize Anti-Stokes shift (up-conversion) efficiently which can convert red to green or blue, another practice would be to use a phosphor that absorb within in visible spectrum like the traditional colored coatings do. This phosphor will provide color to the coating similar to metallic resonators and dyes which absorb in the visible spectrum. However, the phosphor will re-emit a portion of the absorbed energy in the near-IR. $Ba_3(PO_4)_2:Mn^{5+}$ is used for this purpose which is excited in the solar spectrum, reemits in the infrared with a QY = 40%[23]. The thermal and visual performance of the fluorescent coating is then compared with the coating colored by silica core, silver shell NPs from[5] with $f_v = 20x10^{-6}$, $D_o = 30$ *nm*, $D_i = 24$ *nm*.

3 Model

To estimate the reflectance of the coating, fluorescence radiative transfer equation[18] (FRTE) is solved.

$$\frac{dI_\lambda}{ds} = -\kappa_\lambda I_\lambda - \sigma_{s,\lambda} I_\lambda + \frac{\sigma_{s,\lambda}}{4\pi} \int_{4\pi} I_\lambda \Phi_\lambda(\Omega', \Omega) d\Omega' + \int_0^\infty \kappa_{f,\lambda'} I_{\lambda'} Y(\lambda', \lambda) d\lambda' \qquad (2)$$

Where I_λ is spectral intensity, κ_λ and $\kappa_{f,\lambda}$ are spectral total absorptance and spectral absorptance by fluorescence, $\sigma_{s,\lambda}$ is spectral scattering coefficient, Φ_λ is phase function, λ is wavelength, Ω is solid

angle and Y is spectral power yield. Here the difference between the well-known RTE and FRTE is the last fluorescent term in Eq. (2). The in-scattering term in RTE is similar with the fluorescent source term although their integration is performed over different parameters, namely solid angle Ω and wavelength λ. The in-scattering term integrate the scattered intensity over all solid angles using dummy solid angle Ω' and determine its contribution to the intensity at the angle of interest Ω by using scattering phase function $\Phi_\lambda(\Omega',\Omega)$. Similarly, fluorescent source term integrate all the absorbed intensity by the fluorescence at all wavelengths over dummy wavelength λ' and determine its contribution to the intensity at the wavelength of interest by spectral power yield term $Y(\lambda', \lambda)$. Y is defined as;

$$Y(\lambda', \lambda) = QY(\lambda')\frac{\lambda'}{\lambda}P_f(\lambda) \tag{3}$$

where

$$P_f(\lambda) = \frac{\mathrm{f}_{fl}(\lambda)}{\int_0^\infty \mathrm{f}_{fl}(\lambda)d\lambda} \tag{4}$$

Here $P_f(\lambda)$ is the probability distribution function which calculates how much of the normalized fluorescent emission, f_{fl}, is at the wavelength of interest, λ. Since QY is defined over number of photons but not energy, it is multiplied by $\lambda'\backslash\lambda$ which comes from photon energy, $h \cdot c\backslash\lambda$. Also as the fluorescent emission is isotropic, fluorescent term in Eq. (2) is independent of the solid angle unlike the in-scattering term. Lastly, unlike regular RTE, absorptance coefficient has two components, fluorescent and non-fluorescent as shown;

$$\kappa_\lambda = \kappa_{f,\lambda} - \kappa_{nf,\lambda} \tag{5}$$

where $\kappa_{nf,\lambda}$ is non-fluorescence absorptance such as absorption by medium and non-fluorescent particles like scatterers.

FRTE is solved by Monte Carlo method. The open-source solver[18] is capable of solving fluorescence problems accurately. In addition to the procedures of classical Monte Carlo method for non-fluorescent cases, in fluorescence application; a random number is calculated and compared with the quantum yield after absorption. If QY is bigger than the number, a ray is re-emitted with a new wavelength determined from the inverse cumulative distribution function. The new photon energy, e_{new}, is also modified by multiplying the old energy, e_{old}, with λ_{old}'\λ_{new}. The remaining energy caused by Stokes shift, e_{old} - e_{new}, is absorbed in the medium. Absorption coefficient, scattering coefficient and refractive index of the medium is updated according to the new wavelength. For non-fluorescent coatings, spectral transmittance and reflectance are independent of incident spectrum whereas for fluorescent coatings it is. Therefore, transmittance and reflectance are 2D tensors that relates incident spectrum to outgoing spectrum. For non-fluorescent coatings (QY = 0) these two quantities are expressed as a diagonal matrix which can be simplified as a vector. Solving RTE provides reflectance and absorptance of the radiative cooling structures.

Calculating thermal performance is done by estimating the net radiative cooling of colored coatings from the calculated absorptance and reflectance. The coating dissipates heat by emitting radiative heat flux, P''_{rad}, and gains heat by absorbing solar power, P''_{solar}, and atmospheric radiation, P''_{atm}. Therefore, the net cooling power reads:

$$P''_{net} = P''_{rad} - P''_{atm} - P''_{solar}. \tag{6}$$

With the help of Kirchhoff's law, $\alpha(\lambda,\Omega)=\varepsilon(\lambda,\Omega)$, components of the net radiative cooling in Eq. (6) can be calculated as;

$$P''_{rad} = \int_{2\pi} \int_{0}^{\infty} I_{bb}(\lambda,T)_{T=T_{sur}}\, \varepsilon(\lambda,\theta)\cos(\theta)\, d\lambda d\Omega \tag{7}$$

$$P''_{atm} = \int_{2\pi} \int_{0}^{\infty} I_{bb}(\lambda, T)_{T=T_{amb}}\, \alpha(\lambda, \theta) \varepsilon_{atm}(\lambda, \theta) \cos(\theta)\, d\lambda d\Omega \quad (8)$$

$$P''_{solar} = \int_{0}^{\infty} I_{Solar}(\lambda)\, \alpha(\lambda, \theta)_{\theta=0} d\lambda \quad (9)$$

where

$$\varepsilon_{atm}(\lambda, \theta) = 1 - t(\lambda)^{1/\cos(\theta)} \quad (10)$$

Here the atmospheric transmittance t(λ) is taken from 32. The column water vapor and air mass are chosen to be 1 mm and 1.5 AM (Air Mass) respectively. I_{solar}, I_{bb}, T_{sur}, T_{amb} are normal direct solar irradiance[33], blackbody intensity, surface and ambient temperatures respectively. Convection effects are not taken into account since both ambient and surface temperatures are 300 K in this study. While finding the emittance at mid-IR, Lewis-Nielson effective medium theory (EMT) is used to calculate effective absorption properties of the coating since it is also valid at high volume fractions where Maxwell-Garnett EMT is not valid. Mid-IR optical properties of the fluorescent materials are hard to find since they are usually used for applications that are in visible or near-IR domain. For CASN effective absorption index of the coating is calculated with the optical data from literature [] however for the rest of the fluorescent materials their contribution to the emittance are neglected by taking their complex refractive index equal to zero.

Last step in the modeling is to estimate color and saturation to determine the visual performance. Estimation of the color and saturation is performed by using CIE standards[34]. Color matching functions relating the spectral reflected intensity and the color are established by CIE. These functions are related to color perception of human eye, i.e., by means of three detectors (cone cells) able to detect red, blue and green color. Using the spectral reflected intensity and the color matching functions, parameters X, Y, Z, which corresponds to coordinates in the CIE color space, can be calculated;

$$X = 100\frac{\int_{360nm}^{830nm} I_{D65}(\lambda)\, R(0,\lambda)\overline{x}(\lambda)d\lambda}{\int_{360nm}^{830nm} I_{D65}(\lambda)\,\overline{y}(\lambda)d\lambda} \quad (11)$$

$$Y = 100\frac{\int_{360nm}^{830nm} I_{D65}(\lambda)\, R(0,\lambda)\overline{y}(\lambda)d\lambda}{\int_{360nm}^{830nm} I_{D65}(\lambda)\,\overline{y}(\lambda)d\lambda} \quad (12)$$

$$Z = 100\frac{\int_{360nm}^{830nm} I_{D65}(\lambda)\, R(0,\lambda)\overline{z}(\lambda)d\lambda}{\int_{360nm}^{830nm} I_{D65}(\lambda)\,\overline{y}(\lambda)d\lambda} \quad (13)$$

Normalized x, y, z parameters can be used to identify the color in chromacity diagram and calculated as;

$$x = \frac{X}{X+Y+Z} \quad (14)$$

$$y = \frac{Y}{X+Y+Z} \quad (15)$$

$$z = \frac{Z}{X+Y+Z} \quad (16)$$

Here, to define the visual performance, saturation S is defined as[35]

$$S = \frac{\sqrt{a^2+b^2}}{\sqrt{a^2+b^2+L^2}}100\% \quad (17)$$

CIE LAB color space parameters lightness, L, redness - greenness, a, and yellowness - blueness, b, are given as

$$L = 116\, f(Y/Y_n) - 16 \quad (18)$$

$$a = 500[f(X/X_n) - f(Y/Y_n)] \quad (19)$$

$$b = 200[f(Y/Y) - f(Z/Z_n)] \quad (20)$$

where

$$f(s) = s^{1/3}\ if\ s > (24/116)^3 \quad (21)$$

$$f(s) = (841/108)s + 16/116\ \ if\ s < (24/116)^3 \quad (22)$$

and X_n=95.047, Y_n=100, Z_n=108.883.

4 Results

Results of the defined problems are presented in the order they appear in the problem statement section. Firstly, non-pigmented thus non-colored simple two layered radiative coatings are investigated to determine the effect of emitter type and thickness on radiative cooling performance. Then, performance of weakly absorbing PFS is evaluated for two different emitters. Next, CASN is embedded into PDMS and the optical and visual performances are investigated with a parametric study and compared with metallic NP embedded colored coatings. Later, the quantum dot embedded PDMS are studied. Effect of scatterers are quantified by varying their concentration along with quantum dot concentration. Lastly, thermal and visual performance of two phosphors to obtain colors like blue which transfers photon between visible and invisible spectrums are investigated. Effect of fluorescence properties such as quantum yield and Stokes shift are quantified.

4.1 Choosing the suitable emitter

The result of the IR emitter study is presented in Figure 7 (a). Outcome shows that PDMS performs better compared to silica when the optimum thickness for each coating is considered. However, since PDMS is more absorptive in the solar spectrum, its radiative cooling performance decreases more rapidly as the thickness increases after the optimal point compared to the silica. For silica, there is a wide plateau around the optimum thickness which provides better thermal performance for thicker configurations. Therefore, PDMS will be preferred over silica if the chosen fluorescent can provide the desired saturation at a thickness lower than 400 μm. If a weakly absorptive

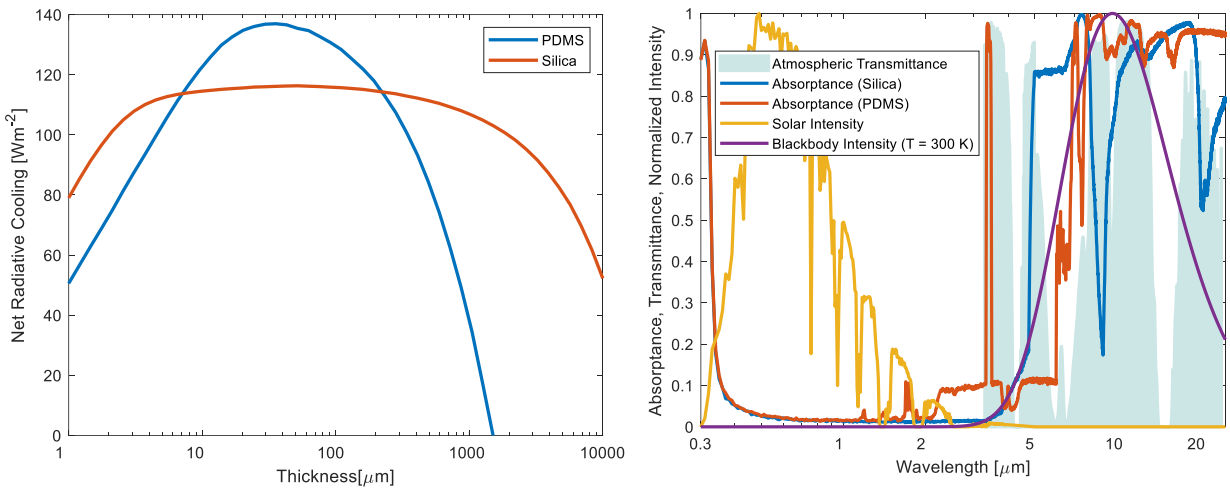

(a) (b)

Figure 7 – (a) Net radiative cooling of PDMS and silica emitter on silver at various thicknesses. (b) Corresponding spectral absorptances of PDMS and silica at 40 μm thickness along with atmospheric transmittance, normalized solar and blackbody intensity at T = 300 K.

fluorescent is chosen and a coating with high saturation is desired, silica is preferable over PDMS. Spectral absorptance value of the coatings with 40 μm thick PDMS and silica emitter along with atmospheric transmittance, solar and blackbody intensities are given in Figure 7 (b). Considering Kirchhoff's law ($\varepsilon_\lambda = \alpha_\lambda$), emittance of PDMS is higher than silica at atmospheric transmittance window, which results a higher thermal performance for PDMS.

4.2 Low-absorbing phosphor

PFS is known for its low absorptivity and its high quantum yield. When we use it as the fluorescence pigment with $f_v = 0.2$, we observe from the results in Figure 8 (a) that the saturation converges to its maximum around 2000 μm thickness which is thicker than the 400 μm limit for PDMS. Therefore, although PDMS performs better for non-colored case, depending on the desired saturation, it could be thermally efficient to use silica emitter instead of PDMS. As the results imply, when the coating is thicker than 400 μm, thermal performance of the coating with silica is

better. When we look at the saturation for a 400 µm thickness, we observe that silica also provides a better coloration. As the thickness increase, saturation of PDMS surpasses silica since absorption in the medium makes the coating look bolder but this also comes with a sharp drop in thermal performance. In case of designs with lighter color, PDMS is preferable over silica since it has a better thermal performance for low thickness. When we observe the spectral flux of the two coatings with 1mm thickness in Figure 8(b) we observe that absorption of PDMS is higher than silica. In addition to resulting a lower thermal performance, high absorption in solar spectrum reduces absorption by fluorescence which slightly decreases the visual performance as it can be observed from reflected fluxes. Under sunlight, PFS powder looks like light yellowish due to its high scattering compared to its absorption. Refractive index mismatch between its surrounding material decreases and high saturation could be observed after it is embedded to silica or PDMS.

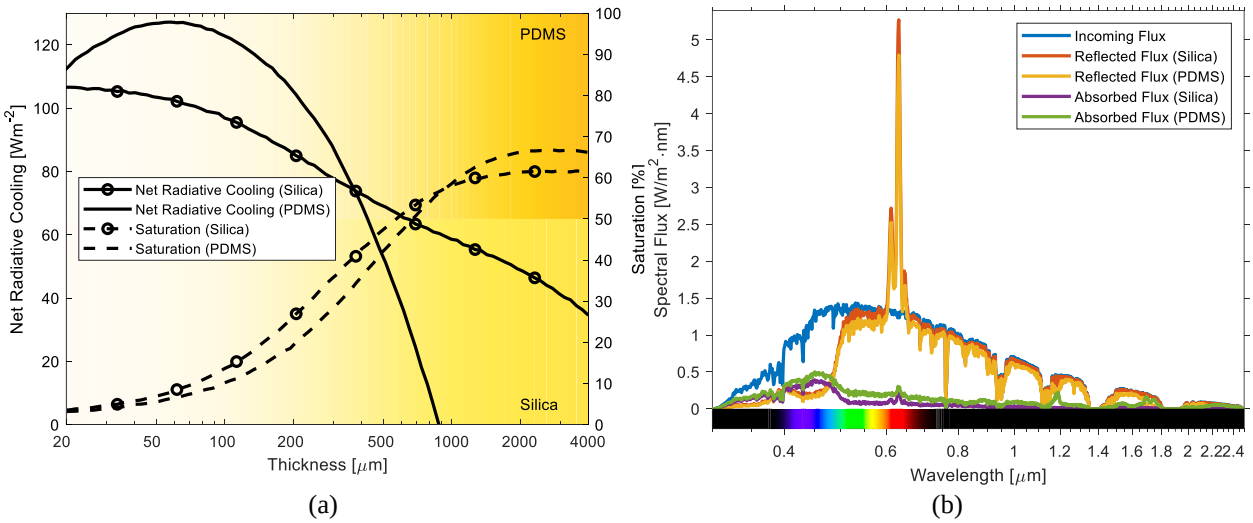

(a) (b)

Figure 8 – (a) Net radiative cooling and saturation of PFS in PDMS and Silica, background correspond to estimated color. (b) Corresponding fluxes of fluorescent coatings with silica and PDMS emitter.

4.3 Down-converting phosphor

Since CASN has a strong absorption, saturation value in Figure 9 (a) shows that color is converged for thicknesses larger than 400 µm. Saturation converges since the available convertible solar

spectrum is already absorbed and converted; further thickening will not provide additional benefit for fluorescence. Since the converged thickness is smaller than 400 μm, use of silica matrix will only lower the thermal performance and therefore avoided.

The colored radiative coating with embedded silver NP is also studied to compare the effect of fluorescence which convert the absorbed light to another spectrum versus the metallic absorbers which transfers the absorbed light to non-radiative energy. We can see from Figure 9 (b) that although the coating with silver NP absorbs in blue to green spectrum and its reflected flux is at red spectrum. The coating with fluorescence also absorbs within blue-green spectrum but convert these photons to red instead of converting to non-radiative energy form, thus outperforms the coating with NPs.

Aforementioned micron sized red phosphor $K2SiF_6:Mn^{4+}$ (PFS), emits red light like CASN under excitation as represented in Figure 3 (b); however, the appearance of the coating with PFS under sunlight is orange unlike the red coating with CASN. The reason is that the excitation spectra of PFS is not as wide as CASN and it does not absorb green part of the sunlight as presented in Figure 3 (a) and Figure 8(b). Thus, despite they emit similar color, the color output of the coatings they are embedded in, show a difference since addition of non-absorbed green light to red makes the coating with PFS orange.

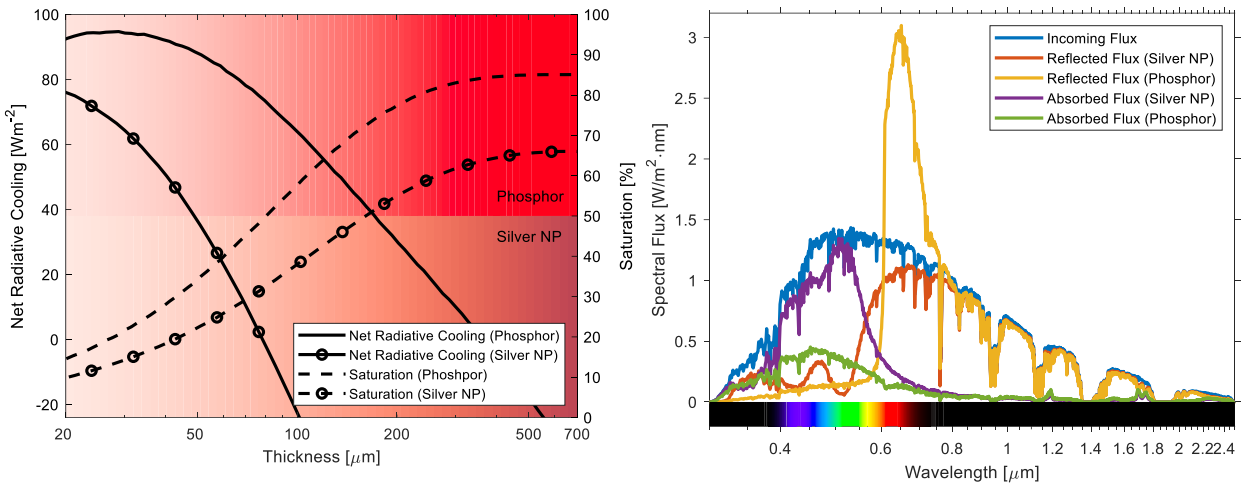

(a) (b)

Figure 9 -(a) Net radiative cooling and saturation of CASN and silver embedded coating, background correspond to estimated color. (b) Corresponding fluxes of the coatings with silver NPs and CASN particles.

4.4 Quantum dots

As mentioned before, since quantum dots are small compared to the wavelengths of the solar spectrum their scattering is in the Rayleigh regime which is negligible compared to their absorption as mentioned before. Fluorescence is isotropic so that all the emitted rays incident on the surface with an angle wider than the critical angle, internally reflects. Since the lower boundary is silver which is a non-ideal reflector, the internally reflected rays are absorbed by silver. As the rays are scattered by micron sized phosphors for the cases investigated so far, prior coatings do not experience this loss. However, the coating with quantum dots does not scatter strongly enough to avoid ray trapping by total internal reflection.

We observe from Figure 10 (a) that increasing scattering concentration increases both visual and thermal performance up to a point where the optimum scatterer amount is observed. Then further increasing the concentration causes a reduction in the thermal performance. Introducing scatterers to the medium helps to avoid ray trapping but it also has destructive effects on thermal performance of the coating. They increase average pathlength of a ray travels inside the coating which increases

solar absorption by the emitter. Moreover, they also absorb the light by themselves. Therefore, the scatterer concentration should be chosen properly with respect to quantum dot concentration. We can observe an increase of thermal efficiency when volumetric scattering concentration increase over 0.01, although saturation does not increase but decrease. Using excess amount of scatterers causes the light to be scattered before they sufficiently interact with quantum dots and reduces the visual performance. If lighter color is desired, instead of using a higher quantum dot and scatterer concentration point such as A, lower scatterer and quantum dot concentration such as B should be chosen as represented on Figure 10 (a). So that 100 Wm^{-2} net cooling power can be obtained instead of 90 Wm^{-2} for the same saturation of 50%.

Same thermal and optical performances can be observed at different concentration mixtures such as point C and D as marked in Figure 10 (a). Choosing D over C could result to use 7 times less quantum dot concentration by implementing cheaper scatterer. The cost reduction by implementing scatterer near to fluorescent pigments was already addressed in the literature[36] before. Here, we observe that it could also be applicable to quantum dot applications. Note also that when we inspect 100 μm thick coating with $3.2x10^{-10}$ mol/L quantum dot without and with scatterers at $fv = 10^{-3}$ from Figure 10 (b), we observe the peak of absorption around 0.5 μm wavelength for without scatterers case because of the trapped and absorbed rays. The absorption difference arises because of the absorption of trapped rays.

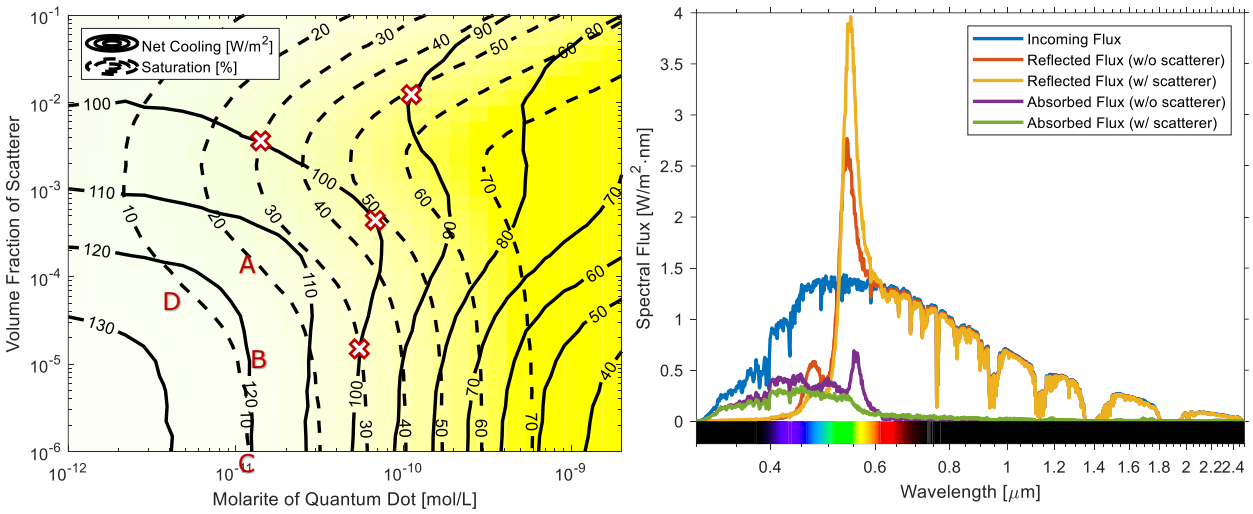

(a) (b)

Figure 10 - (a) Net radiative cooling and saturation of quantum dot and TiO2 scatterer embedded coating, background correspond to estimated color. (b) Corresponding fluxes of the coatings with and without scatterer.

4.5 Conversion between non-visible to visible spectrums

Silver is an effective reflector but it still absorbs highly in the UV spectrum as it can be observed in Figure 7 (b). BAM:Eu phosphor, that absorbs in the invisible UV and emitting at blue is presented in Figure 3, is used in the PDMS coating. We can see in Figure 11 (a) that the saturation is low and the resulting blue has low saturation which cannot be improved by increasing thickness. As we can observe from Figure 11 (b) UV intensity with respect to visible spectrum intensity on the earth surface is not powerful enough to create a blue peak which can suppress the dominance of green, yellow and red spectrum of the sun. Although a phosphor with high quantum yield (95%) is used, moving less efficiently reflectible UV spectrum to more efficiently reflectable blue spectrum does not increase but decrease the thermal performance due to losses from Stokes shift.

Phosphors can also be used to provide color to the coating as non-fluorescent dyes and metallic NPs do. Chosen fluorescent material, $Ba_3(PO_4)_2$:Mn^{5+}, absorbs the radiation in the orange and red

spectrum and emits in the near-IR as presented in Figure 3 (a) and (b) respectively. When we look at

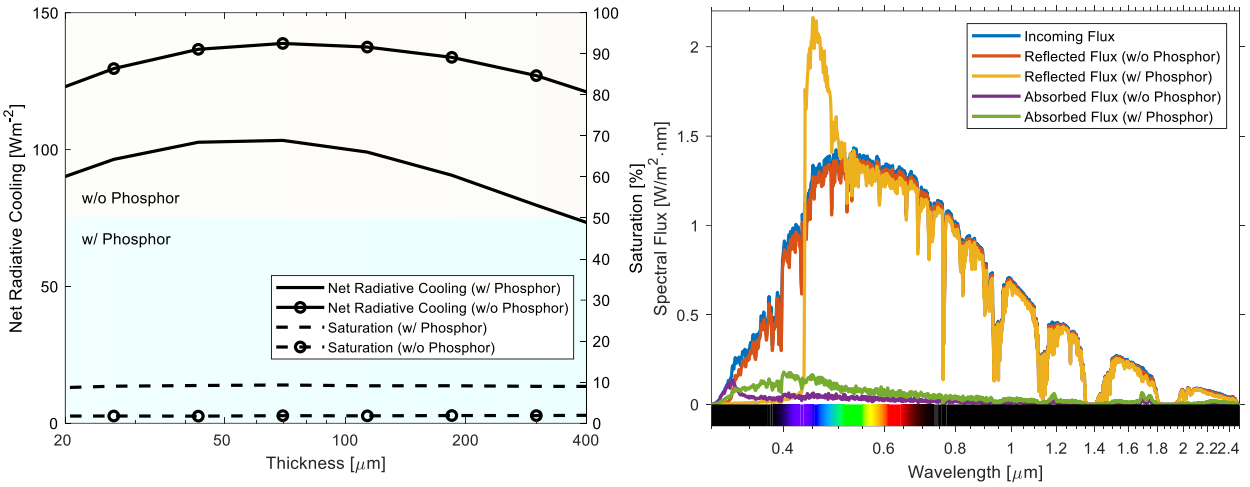

(a) (b)

Figure 11 - (a) Net radiative cooling and saturation of BAM:Eu phosphor embedded coating, background correspond to estimated color. (b) Corresponding fluxes of the coatings with and without phosphor.

the results in Figure 12 (a) and compare the phosphor with silver NP, we observe that the coating with metallic NPs provides better thermal performances. There are three reasons behind the performance differences. The main reason is, metallic NPs exhibit a sharp absorption peak that is tunable by varying their size however the phosphor absorbs broadly as seen in Figure 12 (b) which is a more costly way to have color in terms of thermal performance. The second and third reasons are the low quantum yield and the larger Stokes shift of the phosphor respectively. For the chosen phosphor, not only the QY is low which creates a performance loss but also emission band is not close to visible radiation. We want higher energy photons to leave the system. As photon energy (hc/λ) is low at larger wavelengths we want the phosphor to emit as as the closer from red spectrum in order to have smaller Stokes shift. To show the effect of QY and Stokes shift, and therefore quantify the effect of fluorescence; 4 case studies with fictitious phosphors whose properties are defined by altering the properties of $Ba_3(PO_4)_2:Mn^{5+}$ are defined in Table 1.

For the Case 1, QY of the phosphor is chosen to be 0, which means it does not show a fluorescent behavior. This case is a baseline that shows what if the coating absorbs light but do not re-emit it as the metallic resonators do. For the Case 2, QY of the phosphor is chosen to be 1 (ideal QY). Emission peak of the phosphor is shifted to left by 370 nm for the Case 3. In the last case 4, both *QY = 1* and emission peak is shifted through visible spectrum by 370 nm. While shifting the emission band, upper visible limit 750 nm is considered, if the emission is shifted further, it interferes with visible spectrum, introduces red light and the available blue mixed with red looks pinkish. Considering the cases 1-4, the changes in fluorescent properties QY and Stokes shift do not have an impact on saturation and color for IR emitting phosphor as seen in Figure 12 (a). We can also observe that, spectral reflected flux in the visible region is the same for all these phosphor cases from Figure 12(b). It is expected because incoming flux is absorbed by the phosphors regardless of fluorescent properties QY and Stokes shift. After the absorption, the absorbed photons are either absorbed for good or re-emitted depending on these properties. Since emission spectrum is not in the visible spectrum, visual performance is not affected. However, it is not the case for thermal performance as we can observe from Table - 1. Here, we can observe the quantitative contribution of the fluorescence. Thickness of the coatings presented in Table - 1 are selected such that each coating results a 36% saturation. Normally, the coatings with silver NPs performs thermally better than the coatings with $Ba_3(PO_4)_2$:Mn^{5+} phosphor for all thicknesses. Decreasing QY to 0 and increasing to 1 have a considerable impact on thermal performance as it changes directly the number of rays leaving the coating which expels energy from the coating. Decreasing Stokes shift (Case 3) while keeping the QY low on the other hand, decreases the thermal performance. Normally we expect a performance increase since Stokes shift shortened; however, new emission peak at near IR is now overlaps with excitation spectrum of the phosphor.

Since QY is low, re-absorption of re-emitted photon occurs multiple times and reduces the thermal efficiency. This shows the importance of avoiding phosphors whose excitation and emission bands overlap especially if they have low QY. Lastly, we observe from Case 4 that, increasing QY and decreasing Stokes shift together boosts the thermal performance of the blue coating and coating provides cooling even for the highest saturation level which is around 50%. When we compare nonfluorescent baseline Case 1 with the Phosphor case in Table - 1 we can see that an additional 60 Wm^{-2} heat flux is emitted away by the fluorescence. We can also see from Case 4 that 220 Wm^{-2} more heat flux compared to Case 1 can be emitted by fluorescence by implementing a more proper fluorescent material for the application. These results show that a proper fluorescent with a closer emission to red and higher QY can provide a better result than coatings with silver NPs however there is no such an available phosphor up to our knowledge.

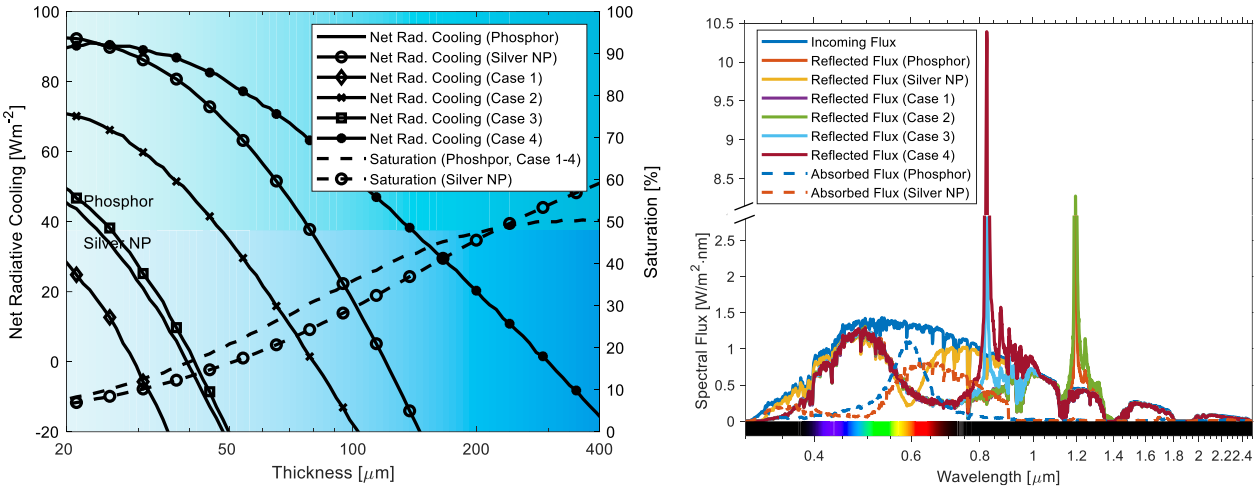

(a) (b)

Figure 12 - (a) Net radiative cooling and saturation of $Ba_3(PO_4)_2:Mn^{5+}$ phosphor embedded coating, background correspond to estimated color. (b) Corresponding fluxes of the coatings with silver NPs and phosphor particles.

Table 1 – Properties of the blue coatings

Coating Name	QY [%]	Stokes Shift [nm]	P_{net} [Wm^{-2}]	Thickness [μm]
Phosphor	40	900	-108	100
Silver NP	0	-	-11	130
Case 1	0	-	-168	100
Case 2	100	900	-19	100
Case 3	40	530	-113	100
Case 4	100	530	52	100

5 Conclusions

We observe that using fluorescent particles instead of non-fluorescent dyes or metallic resonators can provide color to the radiative cooling coating with a lower thermal performance loss. Photoluminescent materials with a higher quantum yield, lower Stokes shift and less overlap between excitation and emission spectrum should be chosen for a better thermal and visual performance. The material used as the emitter of the coating should be selected regarding the desired saturation and absorptance of the phosphor. Varying the color and obtaining a wide color gamut with metallic NPs and nanolayers is possible by varying resonator size as we had shown in our previous studies; however, fluorescence pigments have characteristic emission and absorption spectra which limits color altering capabilities. Using quantum dots can provide efficient radiative cooling with color; however, a proper scatterer with proper concentration should be implemented to the coating. Finally, obtaining colors under sunlight at the high energy region of the visible spectrum such as purple, blue and green is harder to achieve due to Stokes shift. Using phosphors to obtain color by absorbing in the visible and emitting in the IR can be less effective than using metallic NPs. Phosphors should have high quantum yield and low Stokes shift otherwise they will perform poorly since fluorescent absorption peaks are not as sharp as metallic resonator absorption peaks.

Disclosures

The authors declare that there is no conflict of interest.

Acknowledgments

This work was partially funded by the French Government program ANR RADCOOL (reference ANR-17-CE06-0002-01) and PAUSE program (Programme national d'aide a l'Accueil en Urgence des Scientifiques en Exil).

Code, Data, and Materials Availability

The codes along with optical properties that calculate radiative cooling power, spectral reflectance and spectral absorptance of the plane parallel coatings with metallic NPs are published at: https://github.com/refetaliyalcin/ColorRCMC

The codes that solve fluorescent radiative transfer equation and calculates spectral reflectance and absorptance of the plane parallel coating are published at: https://github.com/refetaliyalcin/monte-carlo-rte-fluorescent-medium

References

1. A. P. Raman et al., "Passive radiative cooling below ambient air temperature under direct sunlight," Nature 515(7528), 540–544, Nature Publishing Group, a division of Macmillan Publishers Limited. All Rights Reserved. (2014) [doi:10.1038/nature13883].
2. K. L. Uemoto, N. M. N. Sato, and V. M. John, "Estimating thermal performance of cool colored paints," Energy Build. 42(1), 17–22 (2010) [doi:10.1016/j.enbuild.2009.07.026].
3. L. Zhu, A. Raman, and S. Fan, "Color-preserving daytime radiative cooling," Appl. Phys. Lett. 103(22), 223902 (2013) [doi:10.1063/1.4835995].
4. Y. Sun and Y. Xia, "Gold and silver nanoparticles: A class of chromophores with colors tunable in the range from 400 to 750 nm," Analyst 128(6), 686 (2003) [doi:10.1039/b212437h].
5. R. A. Yalçın et al., "Colored Radiative Cooling Coatings with Nanoparticles," ACS Photonics 7(5), 1312–1322 (2020) [doi:10.1021/acsphotonics.0c00513].

6. E. Blandre et al., “Microstructured surfaces for colored and non-colored sky radiative cooling,” Opt. Express 28(20), 29703 (2020) [doi:10.1364/OE.401368].
7. W. Li et al., “Photonic thermal management of coloured objects,” Nat. Commun. 9(1), 4240 (2018) [doi:10.1038/s41467-018-06535-0].
8. S. Son et al., “Colored emitters with silica-embedded perovskite nanocrystals for efficient daytime radiative cooling,” Nano Energy 79, 105461 (2021) [doi:10.1016/j.nanoen.2020.105461].
9. P. Yu et al., “Temperature-Dependent Fluorescence in Carbon Dots,” J. Phys. Chem. C 116(48), 25552–25557 (2012) [doi:10.1021/jp307308z].
10. T.-C. Liu et al., “Temperature-dependent photoluminescence of water-soluble quantum dots for a bioprobe,” Anal. Chim. Acta 559(1), 120–123 (2006) [doi:10.1016/j.aca.2005.11.053].
11. Y.-H. Won et al., “Highly efficient and stable InP/ZnSe/ZnS quantum dot light-emitting diodes,” Nature 575(7784), 634–638 (2019) [doi:10.1038/s41586-019-1771-5].
12. J. R. Howell and M. Perlmutter, “Monte Carlo Solution of Thermal Transfer Through Radiant Media Between Gray Walls,” J. Heat Transfer 86(1), 116 (1964) [doi:10.1115/1.3687044].
13. F. Asllanaj et al., “Radiative transfer equation for predicting light propagation in biological media: comparison of a modified finite volume method, the Monte Carlo technique, and an exact analytical solution,” J. Biomed. Opt. 19(1), 015002 (2014) [doi:10.1117/1.JBO.19.1.015002].
14. X. Yu et al., “Dynamic Phosphor Sedimentation Effect on the Optical Performance of White LEDs,” IEEE Photonics Technol. Lett. 29(14), 1195–1198 (2017) [doi:10.1109/LPT.2017.2712280].
15. M.-A. A. Mycek and B. W. Pogue, Handbook of Biomedical Fluorescence, in Middle East, CRC Press (2003) [doi:10.1201/9780203912096].
16. A. Liemert, D. Reitzle, and A. Kienle, “Analytical solutions of the radiative transport equation for turbid and fluorescent layered media,” Sci. Rep. 7(1), 3819 (2017) [doi:10.1038/s41598-017-02979-4].

17. R. A. Yalçın and H. Ertürk, “Monte Carlo method solution of the broadband fluorescent radiative transfer equation considering fluorescent cascade,” Appl. Opt. 60(4), 1068 (2021) [doi:10.1364/AO.410325].
18. R. A. Yalcin, “monte carlo rte fluorescent medium,” 2021, <https://github.com/refetaliyalcin/monte-carlo-rte-fluorescent-medium> (accessed 28 April 2021).
19. P. Pust et al., “Narrow-band red-emitting Sr[LiAl3N4]:Eu2+ as a next-generation LED-phosphor material,” Nat. Mater. 13(9), 891–896 (2014) [doi:10.1038/nmat4012].
20. K. Du et al., “The rate equation based optical model for phosphor-converted white light-emitting diodes,” J. Phys. D. Appl. Phys. 50(9), 095101 (2017) [doi:10.1088/1361-6463/aa560a].
21. Y. Kim et al., “Bright and Uniform Green Light Emitting InP/ZnSe/ZnS Quantum Dots for Wide Color Gamut Displays,” ACS Appl. Nano Mater. 2(3), 1496–1504 (2019) [doi:10.1021/acsanm.8b02063].
22. T. Jüstel et al., “Blue emitting BaMgAl10O17:Eu with a blue body color,” J. Lumin. 104(1–2), 137–143 (2003) [doi:10.1016/S0022-2313(03)00010-3].
23. R. Cao et al., “Near-infrared emission Ba3(PO4)2:Mn5+ phosphor and potential application in vivo fluorescence imaging,” Spectrochim. Acta Part A Mol. Biomol. Spectrosc. 128, 671–673 (2014) [doi:10.1016/j.saa.2014.02.081].
24. H. U. Yang et al., “Optical dielectric function of silver,” Phys. Rev. B 91(23), 235137 (2015) [doi:10.1103/PhysRevB.91.235137].
25. R. Kitamura, L. Pilon, and M. Jonasz, “Optical constants of silica glass from extreme ultraviolet to far infrared at near room temperature,” Appl. Opt. 46(33), 8118 (2007) [doi:10.1364/AO.46.008118].
26. L. Zhou et al., “A polydimethylsiloxane-coated metal structure for all-day radiative cooling,” Nat. Sustain. 2(8), 718–724 (2019) [doi:10.1038/s41893-019-0348-5].

27. J. E. Murphy et al., “PFS, K 2 SiF 6 :Mn 4+ : the Red-line Emitting LED Phosphor behind GE’s TriGain TechnologyTM Platform,” SID Symp. Dig. Tech. Pap. 46(1), 927–930 (2015) [doi:10.1002/sdtp.10406].
28. M. G. Brik and A. M. Srivastava, “Ab Initio Studies of the Structural, Electronic, and Optical Properties of K2SiF6 Single Crystals at Ambient and Elevated Hydrostatic Pressure,” J. Electrochem. Soc. 159(6), J212 (2012) [doi:10.1149/2.071206jes].
29. H. F. Sijbom et al., “K2SiF6:Mn4+ as a red phosphor for displays and warm-white LEDs: a review of properties and perspectives,” Opt. Mater. Express 7(9), 3332 (2017) [doi:10.1364/OME.7.003332].
30. E. Jang et al., “Environmentally Friendly InP-Based Quantum Dots for Efficient Wide Color Gamut Displays,” ACS Energy Lett. 5(4), 1316–1327 (2020) [doi:10.1021/acsenergylett.9b02851].
31. R. Toufanian et al., “Engineering Brightness-Matched Indium Phosphide Quantum Dots,” Chem. Mater. 33(6), 1964–1975 (2021) [doi:10.1021/acs.chemmater.0c03181].
32. “Gemini Observatory, IR Transmission Spectra.,” <https://www.gemini.edu/sciops/telescopes-and-sites/observing-condition-constraints/ir-transmission-spectra> (accessed 15 May 2019).
33. NREL, “Solar Spectral Irradiance: Air Mass 1.5,” <http://rredc.nrel.gov/solar/spectra/am1.5/>.
34. H. S. Fairman, M. H. Brill, and H. Hemmendinger, “How the CIE 1931 color-matching functions were derived from Wright-Guild data,” Color Res. Appl. 22(1), 11–23 (1997) [doi:10.1002/(SICI)1520-6378(199702)22:1<11::AID-COL4>3.0.CO;2-7].
35. E. Lubbe, Colours in the Mind - Colour Systems in Reality : A formula for colour saturation, Books On Demand (2010).
36. S. L. Hsiao, N. C. Hu, and C. C. Wu, “Reducing the required amount of phosphor in warm white-light-emitting diodes by enhancing the scattering effect of wavelength conversion layer: A simulation study,” Appl. Phys. Express 6(3) (2013) [doi:10.7567/APEX.6.032102].

Caption List

Fig. 1 Colored radiative cooling coating applied on the roof

Fig. 2 Sketch of the simple two-layer coating.

Fig. 3 (a) Excitation and (b) emission spectrum of the CASN[19], PSF[20], InP/ZnSe/ZnS[21], BAM:Eu[22] and $Ba_3(PO_4)_2$:Mn^{5+}[23].

Fig. 4 Sketch of the simple two-layer coating embedded with phosphor.

Fig. 5 Sketch of the two-layer coating with scatterer and quantum dots along with tracing of a ray emitted by quantum dot.

Fig. 6 Solar spectrum averaged single scattering albedo of TiO_2 and ZnO particles in PDMS..

Fig. 7 (a) Net radiative cooling of PDMS and silica emitter on silver at various thicknesses. (b) Corresponding spectral absorptances of PDMS and silica at 40 μm thickness along with atmospheric transmittance, normalized solar and blackbody intensity at T = 300 K.

Fig. 8 (a) Net radiative cooling and saturation of PFS in PDMS and Silica, background correspond to estimated color. (b) Corresponding fluxes of fluorescent coatings with silica and PDMS emitter.

Fig. 9 (a) Net radiative cooling and saturation of CASN and silver embedded coating, background correspond to estimated color. (b) Corresponding fluxes of the coatings with silver NPs and CASN particles.

Fig. 10 (a) Net radiative cooling and saturation of quantum dot and TiO2 scatterer embedded coating, background correspond to estimated color. (b) Corresponding fluxes of the coatings with and without scatterer.

Fig. 11 (a) Net radiative cooling and saturation of BAM:Eu phosphor embedded coating, background correspond to estimated color. (b) Corresponding fluxes of the coatings with and without phosphor.

Fig. 12 (a) Net radiative cooling and saturation of $Ba_3(PO_4)_2:Mn^{5+}$ phosphor embedded coating, background correspond to estimated color. (b) Corresponding fluxes of the coatings with silver NPs and phosphor particles.

Table 1 Properties of the blue coatings.